Journal of Non-Crystalline Solids 355 (2009) 1–5

Contents lists available at ScienceDirect

Journal of Non-Crystalline Solids

journal homepage: www.elsevier.com/locate/jnoncrysol

Kinetics of Mg_6Ni nanocrystallization in amorphous $Mg_{83}Ni_{17}$

T. Spassov [a,*], St. Todorova [a], V. Petkov [b]

[a] Department of Chemistry, University of Sofia "St.Kl.Ohridski", 1 J. Bourchier str., 1164 Sofia, Bulgaria
[b] Deptartment of Physics, Dow 203, Central Michigan University, Michigan, USA

ARTICLE INFO

Article history:
Received 5 July 2007
Received in revised form 22 September 2008
Available online 14 November 2008

PACS:
61.43.Dq
65.60.+a
81.05.Kf
64.70.dg

Keywords:
Amorphous metals, metallic glasses
Crystallization
Thermal properties

ABSTRACT

A comprehensive crystallization kinetics study was carried out in order to understand the mechanism of formation of a Mg-rich nanocrystalline Mg_6Ni phase in a metallic glass with similar overall composition, $Mg_{83}Ni_{17}$. Adequate description of the transformation kinetics was obtained by the JMKA equation with an integer Avrami exponent $n = 4$, associated with nucleation and three-dimensional linear growth crystallization mechanism. To study the nanocrystals growth mechanism separately a controlled heat treatment of the amorphous alloy was applied and thus a three-dimensional growth with a constant rate was obtained ($n = 3$) for the pre-annealed alloys. For all transformation curves the dependence of n on the degree of transformation α, $n(\alpha)$, was analyzed and the regions with constant n were defined. The correct separation of the processes of nucleation and crystal growth allowed reliable values for the activation energies of both nucleation and growth processes to be determined.

1. Introduction

The thermal stability and crystallization of Mg–Ni-based metallic glasses have been intensively studied [1–6] due to their applicability for hydrogen storage as well as because of the possibility to produce nanocrystalline microstructures with attractive chemical and physical properties. The crystallization, microstructure and hydriding properties of magnesium rich Mg–Ni amorphous alloys with various compositions have been investigated as well [3,6–11]. Depending on the amorphous alloy composition different crystallization mechanisms (eutectic, primary, polymorphous) were determined [2–5,12,13]. Formation of a metastable Mg_6Ni phase with cubic structure (F43m) with high thermal stability was found in Mg-richer Mg–Ni and Mg–Ni–RE alloys [3,5,6]. It has to be pointed out that according to Sommer et al. [5] the composition of the metastable phase is slightly different, i.e. $Mg_{\sim 5.5}Ni$. The formation of Mg_6Ni is inhibited by the increase of the hydrogen concentration introduced into the ribbon [3,6]. During continuous heating this metastable phase transforms to the equilibrium αMg and Mg_2Ni [3]. The thermal stability of the Mg_6Ni phase was found to depend on the alloy composition, as the highest transformation temperature of about 350 °C was detected for $Mg_{83}Ni_{17}$ and $Mg_{87}Ni_{12}Y_1$ [3,13].

The crystallization of the metastable Mg_6Ni phase in amorphous $Mg_{83}Ni_{17}$ alloy was studied and a nucleation with subsequent three-dimensional crystal growth mechanism was found [13]. The activation energy of this transformation, determined by the Kissinger method, was estimated to be 160 ± 10 kJ/mol. An average grain size of about 30 nm was determined before the transformation of this phase to the equilibrium αMg and M_2Ni [13]. In contrast, annealing of the $Mg_{82}Ni_{18}$ amorphous alloy leads to the formation of Mg_2Ni and Mg [5]. The crystallization of this glass is governed by nucleation and three-dimensional growth mechanism [5].

Based on a comprehensive crystallization kinetics analysis the present study aims to elucidate upon the Mg_6Ni nanocrystallization reaction mechanism in a glass with an overall composition very close to Mg_6Ni (i.e. $Mg_{83}Ni_{17}$).

2. Experimental part

The alloy was prepared by melting of high purity Mg (99.95) and Ni (99.99) in an induction furnace under pure argon atmosphere. From the master alloy ingots ribbons were produced by melt-spinning with an approximate quenching rate of 25–30 m/s. The chemical composition of the alloys was examined by SEM with an energy dispersive X-ray analysis (EDX).

The microstructure of the melt-spun materials as well as the crystalline phases in the as-quenched and heat treated alloys were

* Corresponding author. Tel.: +359 2 81 61 236.
E-mail address: tspassov@chem.uni-sofia.bg (T. Spassov).

0022-3093/$ - see front matter © 2008 Elsevier B.V. All rights reserved.
doi:10.1016/j.jnoncrysol.2008.09.038

characterized by X-ray diffraction (XRD) using both in house equipment (Cu-Kα; $\lambda = 1.54$ Å) and synchrotron radiation X-rays ($\lambda = 0.103$ Å) at the beamline 11IDB (Argonne National Laboratory). Thanks to the high energy/short wavelength of synchrotron radiation X-rays used XRD data were collected over quite a wide region (0–25 Å^{-1}) of reciprocal space vectors, Q. Here $Q = 4\pi\ (\sin\theta)/\lambda$, where θ is half the angle between the incoming and outgoing X-rays, and λ is the wavelength of the radiation used. Besides, the higher flux of synchrotron radiation X-rays and the usage of a large area detector yielded XRD data of a very good statistical accuracy. Experimantal struture functions are shown in Fig. 1(a), and their Fourier transforms – the experimental reduced atomic distribution functions, $G(r)$ – in Fig. 1(b).

Thermal stability and crystallization kinetics of the rapidly solidified alloys were studied by means of DSC (Perkin–Elmer DSC7) under pure argon atmosphere.

3. Results and discussion

As already mentioned in the introduction, in a series of our previous studies [3,4,12,13] the formation of the metastable Mg_6Ni phase in melt-spun amorphous Mg–Ni alloys was analyzed. The kinetics of its formation and its thermal stability depend on the amorphous alloy composition. For the one with an overall composition close to that of the metastable Mg_6Ni compound ($Mg_{83}Ni_{17}$) the kinetic analysis reveals nucleation with subsequent three-dimensional linear growth mechanism [13], although the microstructure of the Mg_6Ni formed is fine nanocrystalline (10–15 nm) and remains in the nanometer range (20–30 nm) during annealing up to the temperatures of its decomposition to αMg and Mg_2Ni (330–360 °C). Substantial grain growth of Mg_6Ni was not detected as well. Therefore, it was challenging to take a deeper look into the local range order of the as-cast amorphous $Mg_{83}Ni_{17}$ alloy. As can be seen in Fig. 1(a) the experimental structure function for as-cast $Mg_{83}Ni_{17}$ exhibits a sharp first peak followed by low-frequency, low-amplitude oscillations, a picture typical for metallic glasses. The $Q[S(Q) - 1]$ data for the Mg_6Ni phase show more and sharper peaks, reflecting the onset of (nano)crystallization. Correspondingly, the correlations between atoms in Mg_6Ni are defined better and extend to longer interatomic distances compared to those seen in as cast $Mg_{83}Ni_{17}$. This is well demonstrated by the fact that the atomic PDF for Mg_6Ni is much more structured than that for amorphous $Mg_{83}Ni_{17}$. (see Fig. 1b) which decays to zero already at approx. 20 Å.

The DSC analysis of the amorphous $Mg_{83}Ni_{17}$ (Fig. 2) shows a single crystallization reaction at 165 °C ($T_{max} = 175$ °C), resulting in nano-Mg_6Ni formation (see Fig. 1), with an enthalpy of crystallization of 70 J/g and confirms our preliminary results [13]. The transformation of the metastable Mg_6Ni phase into the equilibrium αMg and Mg_2Ni takes place with a low velocity in the temperature range of 300–350 °C and therefore the thermal peak associated with this reaction is very broad and weak. Compared to other Mg based metallic glasses, which also transform to the stable crystalline state through the metastable Mg_6Ni phase, the thermal stability of the Mg_6Ni phase in the studied alloy is higher.

It is interesting to note that the Mg_6Ni phase, formed by annealing the $Mg_{83}Ni_{17}$ glass up to a temperature immediately after the single crystallization peak (180 °C), is extremely fine nanocrystalline (3–4 nm). Experimental XRD and RDF data clearly show that the short-range atomic order in the nanocrystallized alloy extends to about 3.0 nm (Fig. 1(b)). In addition, the (nano)crystallization involves a modification/change of the immediate/local atomic/chemical order in the glass as indicated by the change in the shape of the first peak in the corresponding atomic RDFs.

To determine the mechanism of the crystallization reaction, leading to the nanocrystalline Mg_6Ni phase, a comprehensive isothermal kinetic study at different temperatures was carried out. Figs. 3 and 4 present the DSC isothermal curves and the corresponding transformation curves in the range 145–165 °C, which is the largest temperature interval in which the reaction kinetics

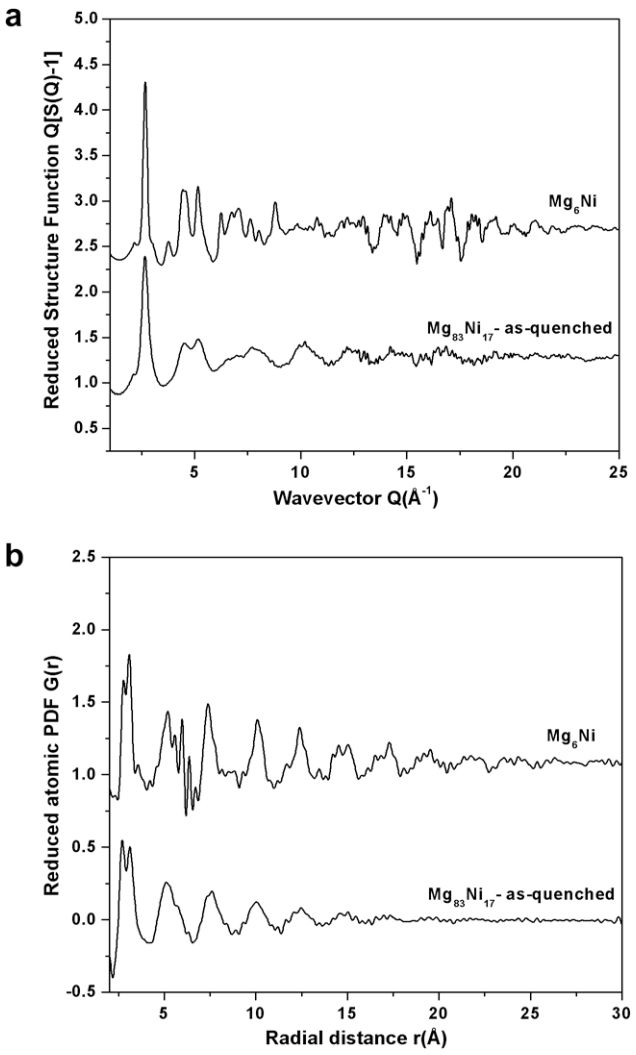

Fig. 1. Experimental structure functions of as-quenched $Mg_{83}Ni_{17}$ and Mg_6Ni phase (a) and their Fourier transforms (b).

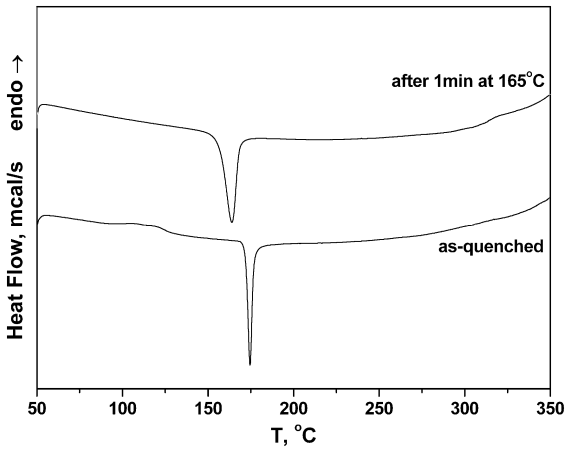

Fig. 2. DSC scans of as-quenched and pre-annealed $Mg_{83}Ni_{17}$.

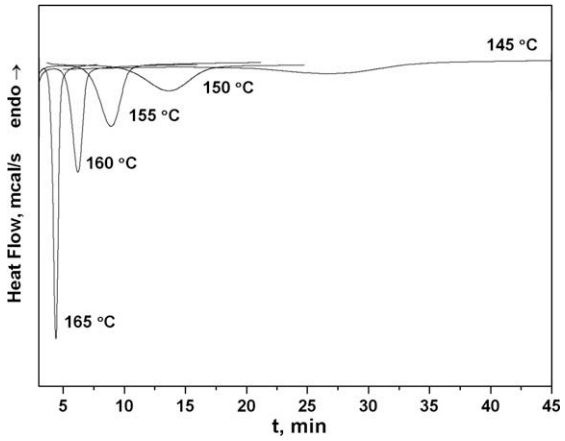

Fig. 3. DSC isotherms of Mg_6Ni crystallization reaction in as-quenched $Mg_{83}Ni_{17}$.

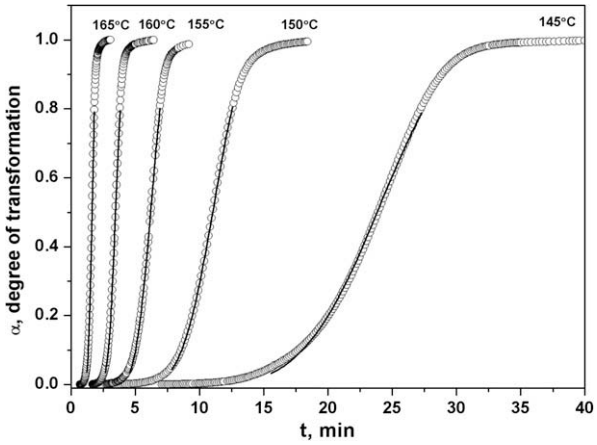

Fig. 4. Corresponding transformation curves of the crystallization of Mg_6Ni in $Mg_{83}Ni_{17}$ (solid line, calculated transformation curves according to the JMKA model with $n = 4$).

can be correctly investigated. Since our preliminary investigation [13] showed a crystallization mechanism (nucleation with subsequent three-dimensional linear growth), which is not typical for a nanocrystallization reaction in metallic glasses, the present study aimed to obtain more information on the transformation mechanism and, if possible, to get reliable results on the nucleation and nanocrystals growth processes separately. From the kinetic curves, plotted in logarithmic coordinates of the JMKA equation, ($\alpha = 1 - \exp(-k(t-\tau_0)^n)$ [14,15], Fig. 5, an average Avrami exponent of $n = 4$ was obtained for all temperatures in the range 150–165 °C. At lower temperatures (145 °C) n is about 3.5, which most probably means that at this temperature growth of pre-existing nuclei proceeds parallel with the nucleation process. It has to be pointed out that at the low temperatures of isothermal annealing (145 and 150 °C) the deviation from the linear dependence is substantial, indicating that at these temperatures a satisfactory prediction of the transformation kinetics by the JMKA model with a constant Avrami exponent n can not be obtained. The incubation time, τ_0, in the JMKA equation was determined from the experimental kinetic curves.

Fig. 4 reveals the non-linear fit of the experimental kinetic curves by JMKA equation at fixed $n = 4$ for $T = 150$, 155, 160 and 165 °C and at $n = 3.5$ for $T = 145$ °C. The kinetic constant in the JMKA equation, estimated at fixed value of $n = 4$, k_4, includes the nucleation (J) and growth (u) rates, according to the equation $k_4 = c \cdot J \cdot u^3$ (c is a constant). Its temperature dependence, Fig. 6, gives the overall activation energy of crystallization $Q = 864 \pm 2$ kJ/mol. It includes the activation energy for nucleation (Q_n) and for three-dimensional crystal growth (Q_g). Although the description of the experimental curves by the JMKA model is very good one can clearly see that there is a noticeable difference between the experimental and calculated curves for $\alpha < 0.1$–0.2, Fig. 4, especially at the lower annealing temperatures.

Due to the observed differences in the values of n, determined using different parts of the $\alpha(t)$ curve, its dependence on the degree of transformation α, $n(\alpha)$, was studied for all experimental curves, Fig. 7, according to the equation: $n(\alpha) = \frac{\partial \ln[\ln(1/(1-\alpha))]}{\partial \ln(t-\tau_0)}$. It is obvious that n varies with α for all temperatures of annealing. At higher temperatures ($\geqslant 155$ °C) after a transient period, in which n increases from 3 to 4–4.5, a nearly constant Avrami exponent, $n = 4.5 \pm 0.2$, was established. These values imply that nucleation and further three-dimensional linear growth is the most probable crystallization mechanism. Values of n above 4 usually reveal a nucleation process with increasing nucleation rate. The transient period, before a constant value of n to be established, varies between $\alpha = 0$–0.20 to $\alpha = 0$–0.30 and depends on the temperature of isothermal annealing, as it is shorter for the higher temperatures. At the lower annealing temperatures (150 °C) n reaches a

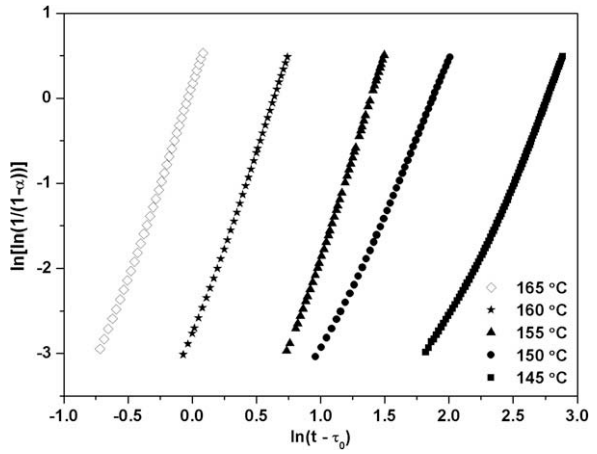

Fig. 5. Kinetic curves, plotted in logarithmic coordinates for the isothermal experiments in the range 145–165 °C.

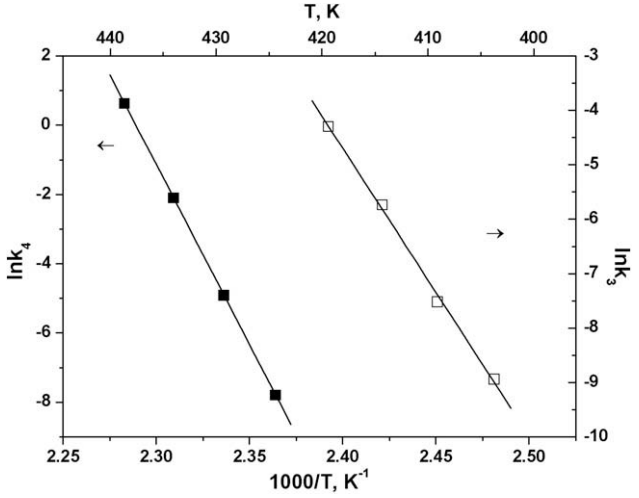

Fig. 6. Arrhenius temperature dependence of the kinetic constant k_4 (for as-quenched $Mg_{83}Ni_{17}$) and k_3 (for the pre-annealed $Mg_{83}Ni_{17}$) in the JMKA equation for the crystallization of Mg_6Ni.

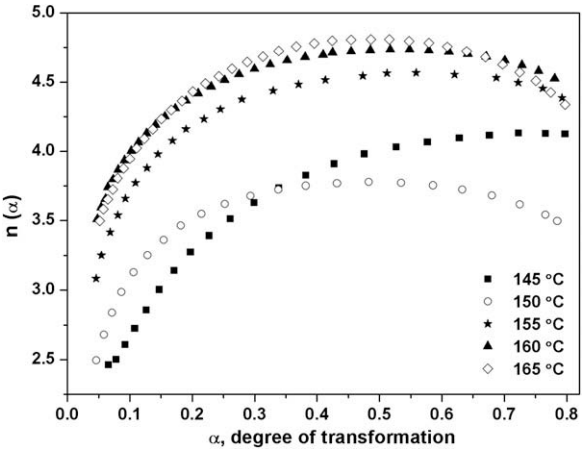

Fig. 7. Dependence of n on the degree of transformation (α) in the range 145–165 °C for the as-quenched $Mg_{83}Ni_{17}$.

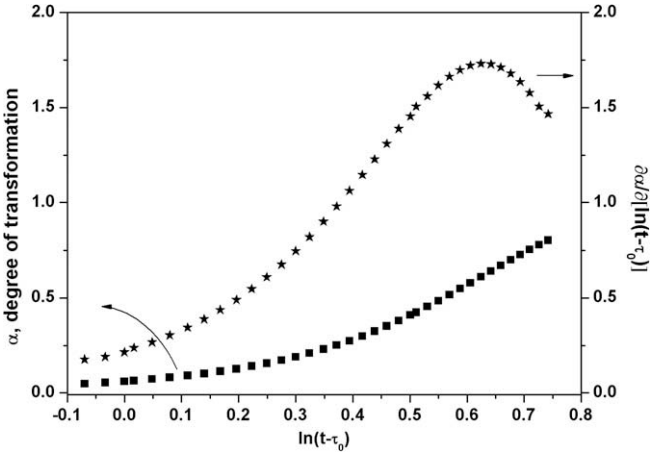

Fig. 8. Dependence of α on $\ln(t-\tau_0)$ (filled squares) and its first derivative (filled stars).

nearly constant value of 3.5 at $\alpha = 0.25$ and remains 3.5 almost until $\alpha \approx 0.7$, which means that the dominating mechanism is three-dimensional linear growth of pre-existing crystal nuclei and simultaneous nucleation with subsequent three-dimensional growth (i.e. both mechanisms work simultaneously). A possible reason for the different shape of the $n(\alpha)$ curve at 145 °C is the poorer precision of the isothermal kinetics analysis at low temperatures, due to the slow release of heat and the resulting option for an incomplete crystallization. The last was detected by a DSC isochronal experiment after isothermal annealing at 145 °C.

Applying the approach of Avramov et al. [16], which uses for the Avrami exponent determination the more reliable experimental data in the middle part of the "$\alpha - t$" curve, similar n-values were obtained (Table 1). According to this approach, for the interpretation of the kinetic results the coordinates "α vs. $\ln(t-\tau_0)$" instead of "α vs. $(t-\tau_0)$" are used, Fig. 8. From the maximum slope ($\alpha' = \frac{\partial\alpha}{\partial[\ln(t-\tau_0)]}$) of the S-shaped curve, Fig. 8, the Avrami exponent n can be determined according to $\alpha' = 0.368.n$ [16]. The n-values obtained by this method depend on the temperature of annealing and correspond to the n-values determined in the range of $\alpha = 0.3$–0.7 (see Fig. 7).

On the basis of the above reported results it can be concluded that the fine nanostructure formed by the crystallization of the studied metallic glass can only result from a high nucleation rate. However, to understand the nanocrystallization reaction in detail it is necessary to study the nucleation and growth reactions separately. To achieve this a short time (1 min) pre-annealing was applied at 165 °C in order to generate sufficient nucleation sites in the amorphous alloy and then the alloy was rapidly cooled down to room temperature. After this pre-annealing of the alloy the crystallization reaction was carried out at different temperatures in the range 130–145 °C, where the process is supposed to be controlled mainly by the crystal growth. The pre-annealing time (1 min) was chosen to correspond to the incubation time of the overall crystallization reaction at this temperature (165 °C). DSC scan of the pre-annealed sample (1 min at 165 °C) shows also an exothermic peak, which differs in its shape from that of the as-cast sample, Fig. 2. The pre-annealing causes a shift in the crystallization temperature to a lower value (from ~165 °C to ~160 °C), but the crystallization enthalpy remains practically equal for both samples (70 J/g for the as-cast and pre-annealed alloys). This result reveals that indeed the pre-annealing most probably results in formation of crystalline nuclei (clusters), which have a negligible volume part in the amorphous matrix. As it was mentioned above the pre-annealed samples were subjected to an isothermal kinetic analysis. In this case the temperature range in which such study could correctly be carried out was 130–145 °C. The experimental DSC curves and the corresponding transformation curves are shown in Fig. 9. From the experimental data in the linearized JMKA coordinates, Fig. 10, an Avrami exponent $n = 3$ was determined for most of the kinetic curves obtained at different temperatures. The Avramov's approach [16] and the non-linear fit of the experimental curves with the JMA equation also give n-values of about 3. These values imply three-dimensional linear growth of existing nuclei, as the most probable crystallization mechanism of the pre-annealed samples.

The $n(\alpha)$-dependence was also derived from the isothermal kinetic curves of the pre-annealed alloys, Fig. 11. The pre-annealed samples show smaller "incubation" period, before a constant n-value to be reached, compared to the as-cast alloys. At $\alpha > 0.1$–0.2, n

Table 1
n-values obtained applying the approach of Avramov et al.

T °C	$\alpha' = n/2.718$	n
145	1.74	4.7
150	1.73	4.7
155	1.67	4.5
160	1.37	3.7
165	1.51	4.1

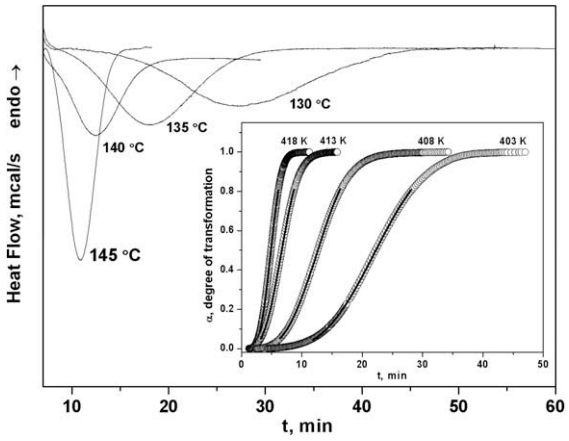

Fig. 9. DSC isotherms and corresponding transformation curves (inset) of the crystallization of Mg_6Ni in pre-annealed $Mg_{83}Ni_{17}$ (solid line, calculated transformation curves according to the JMKA model with $n = 3$).

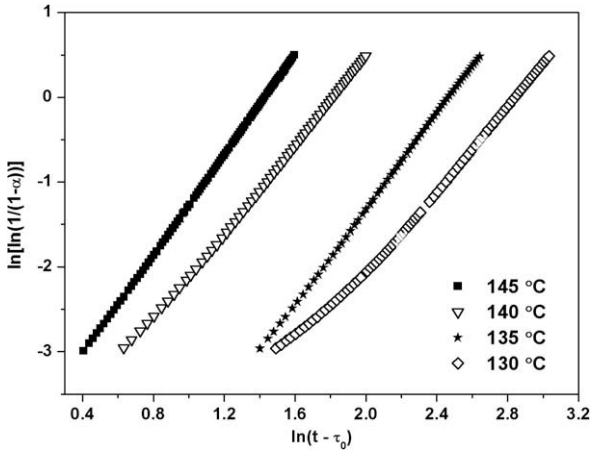

Fig. 10. Kinetic curves, plotted in logarithmic coordinates for the isothermal experiments in the range 130–145 °C.

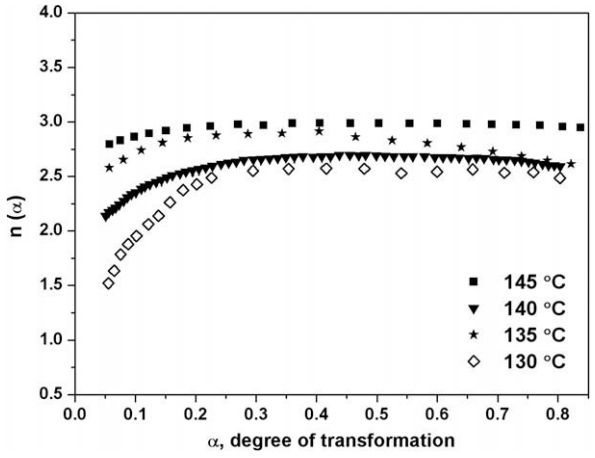

Fig. 11. Dependence of n on the degree of transformation (α) in the range 130–145 °C for the pre-annealed $Mg_{83}Ni_{17}$ samples.

obtains a constant value of 2.5–3.0, depending on the temperature of annealing. It is noteworthy that at 145 °C n possesses an almost exact value of 3 in the whole range of α.

From the temperature dependence of the k_3-values (the kinetic constant in the JMKA equation at $n = 3$; $k_3 = c \cdot N \cdot u^3$, where N is the number of nuclei formed during the pre-annealing (1 min/165 °C)) the activation energy of three-dimensional crystal growth was obtained, $Q_g = 440 \pm 15$ kJ/mol (Fig. 6), because in the constant k_3 only the growth rate u is temperature dependant.

The extrapolation of the k_3-values to higher temperatures, at which the crystallization kinetics of the as-quenched samples were studied (150–165 °C), enables analyzing of the temperature dependence of the nucleation rate $J(T)$, according to the equation: $k_4(T)/k_3(T) = J(T)/N$. From the Arhenius temperature dependence of $k_4(T)/k_3(T)$, Fig. 12, the activation energy of nucleation, $Q_n = 423 \pm 2$ kJ/mol, was determined. This value is noticeably lower compared to that for nucleation processes in other metallic glasses and could explain the high nucleation rate in this alloy [17,18].

4. Conclusions

On the base of comprehensive crystallization kinetics study the mechanism of nanocrystallization of Mg_6Ni in the $Mg_{83}Ni_{17}$ glass was determined. A nucleation and three-dimensional linear growth crystallization mechanism was found for the as-quenched amorphous alloy. The process of nanocrystals growth was studied separately by applying a controlled pre-annealing of the glass. Thus, a three-dimensional growth with a constant rate was obtained for the pre-annealed alloys. The correct separation of the processes of nucleation and crystal growth allowed reliable values for the activation energies of both nucleation and growth to be obtained.

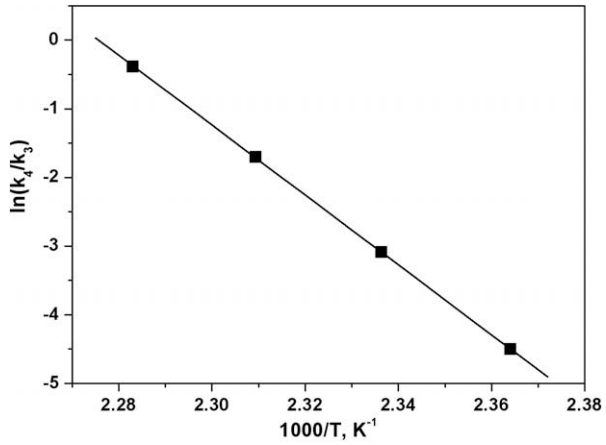

Fig. 12. Arrhenius temperature dependence of $k_4(T)/k_3(T)$ (filled squares) and its linear fit (solid line).

Acknowledgements

The work has been supported by the Bulgarian Scientific Research Fund under grant BYX-14/05 and by the National Science Fund, Project "University research center on nanotechnologies and new materials". Use of the Advanced Photon Source was supported by the US Department of Energy, Office of Basic Energy Sciences, under Contract DE-AC02-06CH11357.

References

[1] A. Inoue, T. Masumoto, Mater. Sci. Eng. A173 (1993) 1.
[2] T. Spassov, U. Köster, J. Alloys Comp. 279 (1998) 279.
[3] T. Spassov, U. Köster, J. Alloys Comp. 287 (1999) 243.
[4] T. Spassov, L. Lybenova, U. Köster, M.D. Baro, Mater. Sci. Eng. A 375–377 (2004) 794.
[5] A.T. Kempen, H. Nitsche, F. Sommer, E.J. Mittemeijer, Metal. Mater. Trans. A 33A (2002) 1041.
[6] A. Teresiak, A. Gebert, M. Savyak, M. Uhlemann, Ch. Mickel, N. Mattern, J. Alloys Comp. 398 (2005) 156.
[7] S. Orimo, H. Fujii, K. Ikeda, Acta Mater. 45 (1997) 331.
[8] S. Orimo, H. Fujii, Appl. Phys. A 72 (2001) 167.
[9] L. Zaluski, A. Zaluska, J.O. Ström-Olsen, J. Alloys Comp. 253&254 (1997) 70.
[10] A. Gebert, B. Khorkounov, U. Wolff, Ch. Mickel, M. Uhlemann, L. Schultz, J. Alloys Comp. 419 (2006) 319.
[11] T. Spassov, V. Rangelova, P. Solsona, M.D. Baró, D. Zander, U. Köster, J. Alloys Comp. 398 (2005) 39.
[12] T. Spassov, V. Rangelova, N. Neykov, J. Alloys Comp. 334 (2002) 219.
[13] T. Spassov, P. Solsona, S. Suriñach, M.D. Baró, J. Alloys Comp. 345 (2002) 123.
[14] A.N. Kolmogorov, Izv. Akad. Nauk USSR. Ser. Matem. 3 (1937) 355.
[15] M.W.A. Johnson, K.F. Mehl, Trans. Am. Inst. Min. Metall. Pet. Eng. 135 (1939) 416.
[16] I. Avramov, K. Avramova, C. Ruessel, J. Cryst. Growth 285 (2005) 394.
[17] A. Pratap, K.G. Raval, A. Gupta, S.K. Kulkarni, Bull. Mater. Sci. 23 (3) (2000) 185.
[18] S. Budurov, T. Spassov, K. Marchev, Wissenschaftliche Berichte "Seminar on Rapid Solidification", Akademie der Wissenschaften der DDR, Dresden, 1988. p. 196..